10306–10320 *Nucleic Acids Research, 2017, Vol. 45, No. 17* *Published online 11 August 2017*
doi: 10.1093/nar/gkx700

Structure of a novel antibacterial toxin that exploits elongation factor Tu to cleave specific transfer RNAs

Karolina Michalska[1,2,†], Grant C. Gucinski[3,†], Fernando Garza-Sánchez[4], Parker M. Johnson[5], Lucy M. Stols[1], William H. Eschenfeldt[1], Gyorgy Babnigg[1], David A. Low[3,4], Celia W. Goulding[5,6], Andrzej Joachimiak[1,2,7,*] and Christopher S. Hayes[3,4,*]

[1]Midwest Center for Structural Genomics, Biosciences Division, Argonne National Laboratory, Argonne, IL 60439, USA, [2]Structural Biology Center, Biosciences Division, Argonne National Laboratory, Argonne, IL 60439, USA, [3]Biomolecular Science and Engineering Program, University of California, Santa Barbara, CA 93106-9625, USA, [4]Department of Molecular, Cellular and Developmental Biology, University of California, Santa Barbara, CA 93106-9625, USA, [5]Department of Molecular Biology and Biochemistry, University of California, Irvine, CA 92697, USA, [6]Department of Pharmaceutical Sciences, University of California, Irvine, CA 92697, USA and [7]Department of Biochemistry and Molecular Biology, University of Chicago, Chicago, IL 60637, USA

Received May 30, 2017; Revised July 26, 2017; Editorial Decision July 27, 2017; Accepted July 29, 2017

ABSTRACT

Contact-dependent growth inhibition (CDI) is a mechanism of inter-cellular competition in which Gram-negative bacteria exchange polymorphic toxins using type V secretion systems. Here, we present structures of the CDI toxin from *Escherichia coli* NC101 in ternary complex with its cognate immunity protein and elongation factor Tu (EF-Tu). The toxin binds exclusively to domain 2 of EF-Tu, partially overlapping the site that interacts with the 3′-end of aminoacyl-tRNA (aa-tRNA). The toxin exerts a unique ribonuclease activity that cleaves the single-stranded 3′-end from tRNAs that contain guanine discriminator nucleotides. EF-Tu is required to support this tRNase activity *in vitro*, suggesting the toxin specifically cleaves substrate in the context of GTP·EF-Tu·aa-tRNA complexes. However, superimposition of the toxin domain onto previously solved GTP·EF-Tu·aa-tRNA structures reveals potential steric clashes with both aa-tRNA and the switch I region of EF-Tu. Further, the toxin induces conformational changes in EF-Tu, displacing a β-hairpin loop that forms a critical salt-bridge contact with the 3′-terminal adenylate of aa-tRNA. Together, these observations suggest that the toxin remodels GTP·EF-Tu·aa-tRNA complexes to free the 3′-end of aa-tRNA for entry into the nuclease active site.

INTRODUCTION

Bacteria have long been known to antagonize one another with soluble antibiotics and bacteriocins (1,2). These compounds diffuse through the environment and inhibit competitors at a distance. More recently, type IV, V, VI and VII secretion systems have been shown to mediate intercellular competition in a contact-dependent manner by delivering toxins directly into neighboring bacteria (3–6). This phenomenon was first described in *Escherichia coli* isolate EC93, which uses its CdiB/CdiA two-partner secretion proteins to bind and inhibit the growth of other *E. coli* strains (3). CdiB is an Omp85 transport protein that exports and assembles the CdiA effector onto the cell surface. CdiA is predicted to form a β-helical filament extending several hundred angstroms from the cell surface. CdiA binds to BamA on neighboring *E. coli* cells, then delivers its C-terminal toxin domain (CdiA-CT) into the target cell to inhibit growth (7,8). Because *E. coli* EC93 cells exchange toxins with neighboring siblings, they protect themselves from self-inhibition by producing a specific contact-dependent inhibition immunity (CdiI) protein that binds and neutralizes toxin. Since its discovery in *E. coli* EC93, *cdi* gene clusters have been identified and characterized in a variety of Gram-negative bacterial pathogens (9–13). Remarkably, CdiA-CT sequences are extraordinarily variable between bacteria, and isolates of the same species commonly deploy different toxins (14,15). Because immunity is conferred through specific protein–protein interactions (16–20), CdiI sequences are also highly variable between bacteria. The diversification of CdiA-CT and CdiI sequences is thought to

*To whom correspondence should be addressed. Tel: +1 805 893 2028; Fax: +1 805 893 4724; Email: chayes@lifesci.ucsb.edu
Correspondence may also be addressed to Andrzej Joachimiak. Tel: +1 630 252 3926; Fax: +1 630 252 6126; Email: andrzejj@anl.gov
†These authors contributed equally to the paper as first authors.

reflect the selective pressure of inter-bacterial competition, with novel toxins conferring a fitness advantage.

In some instances, CdiA-CT domains require additional factors to promote toxic activity. For example, CdiA-CT^{EC536} from uropathogenic *E. coli* 536 is a potent tRNA anticodon nuclease *in vivo* (9), but the purified toxin has no RNase activity *in vitro* (21). CdiA-CT^{EC536} is activated when it binds to CysK, an *O*-acetylserine sulfhydrylase that catalyzes the final step in L-cysteine biosynthesis. CysK stabilizes the toxin fold and promotes interactions with tRNA substrates (19,21). Another CDI tRNase toxin from *E. coli* strain EC869 forms a high-affinity complex with elongation factor Tu (EF-Tu) (22). EF-Tu is an essential and highly conserved translation factor that delivers aminoacyl-tRNAs (aa-tRNA) to the ribosome during protein synthesis. CdiA-CT^{EC869} nuclease activity requires both EF-Tu and GTP, suggesting that GTP·EF-Tu·aa-tRNA ternary complexes are the physiologically relevant substrates (22). Genetic evidence from this latter study indicates that unrelated CDI toxins from *E. coli* isolates 96.154 and NC101 might also interact with EF-Tu. Here, we present structural and biochemical data that confirm the functional interaction between CdiA-CT^{NC101} and EF-Tu. Structures of the EF-Tu·CdiA-CT·CdiI^{NC101} ternary complex reveal that the toxin binds EF-Tu at a site that partially overlaps with the aa-tRNA binding site. The toxin domain adopts the barnase/EndoU/colicin E5-D/RelE (BECR) RNase fold (23), and cleaves the single-stranded 3′-end of tRNAs that contain a guanine discriminator nucleotide. Because EF-Tu is required for this unusual nuclease activity, the toxin presumably recognizes substrate in the context of GTP·EF-Tu·aa-tRNA ternary complexes. However, superimposition of the toxin onto GTP·EF-Tu·aa-tRNA indicates that the nuclease active site is ∼12 Å from the scissile phosphodiester bond. Moreover, there are several predicted steric clashes between the 3′-end of aa-tRNA and EF-Tu bound toxin. We propose that CdiA-CT^{NC101} disrupts contacts between aa-tRNA and EF-Tu, thereby freeing the 3′-end of tRNA for toxin-mediated cleavage.

MATERIALS AND METHODS

Plasmid constructions and site-directed mutagenesis

Plasmids and oligonucleotides are listed in Supplementary Tables S1 and S2, respectively. The coding sequence for residues Val3035—Lys3289 of CdiA^{NC101} (locus tag ECNC101_RS22895) and CdiI^{NC101} (ECNC101_RS22895) from *E. coli* NC101 was synthesized by Genscript and supplied in plasmid pUC57. For crystallographic studies, the *cdiA-CT*/*cdiI*^{NC101} module was amplified with primer pair PSI-1/PSI-2. The forward primer adds a 5′ ligation-independent cloning (LIC) sequence and an ATG start codon to the toxin coding sequence, and the reverse primer adds the 3′ LIC region coding for a short linker and the first two amino acids of the His_6-tag to the CdiI coding sequence (24). The polymerase chain reaction (PCR) product was gel-purified, treated with T4 DNA polymerase and dTTP (25) and cloned into expression vector pMCSG58 (24) according to ligation-independent procedures (26,27). The resulting construct pMCSG58-CPX200205 was confirmed by DNA sequencing and transformed into *E. coli* BL21(DE3)-Gold cells for over-expression.

For biochemical and *in vivo* activity analyses, the *cdiA-CT*/*cdiI*^{NC101} module was amplified with primers CH3880/CH3239 and CH3269/CH3422 and the resulting fragments introduced into pCH10068 and pCH7171 to generate plasmids pCH12641 and pCH12598, respectively. Site-directed mutagenesis of the *cdiA-CT*^{NC101} coding sequence was performed by mega-primer PCR or the QuikChange II Site-Directed Mutagenesis Kit (Stratagene) according to manufacturer's instructions. The *cdiI*^{NC101} gene was amplified with primers CH3238/CH3422 and ligated to pET21 using KpnI/SpeI restriction sites to generate plasmid pCH12745 for the purification of CdiI^{NC101}-His_6. The *E. coli cca* gene encoding tRNA nucleotidyltransferase was amplified with primers CH4062/CH4063 and ligated to pET21 using KpnI/XhoI restrictions sites to generate plasmid pCH13076.

The chimeric *cdiA*^{EC93}-*CT*^{NC101} expression construct (pCH11434) has been described previously (28). Site-directed mutant forms of this plasmid were constructed by allelic exchange of the counter-selectable *pheS** marker from plasmid pCH10163 (16). *cdiA-CT*/*cdiI*^{NC101} sequences were amplified with primers CH3176/CH3177 and fused to DNA fragments amplified from regions upstream and downstream of the *cdiA*^{EC93} gene. The upstream homology fragment was amplified using primers CH4100/CH4101, and the downstream fragment with primers CH4102/CH4103. The three products were then fused to each other by overlap-extension PCR (OE-PCR) using primers CH4100/CH4103. The final DNA product (100 ng) was electroporated together with plasmid pCH10163 (300 ng) into *E. coli* DY378 cells (29). Recombinant plasmid clones were selected on yeast extract glucose-agar supplemented with 33 μg/ml chloramphenicol and 10 mM D/L-*p*-chlorophenylalanine. All constructs were confirmed by DNA sequence analysis.

Protein purification and crystallization

The CdiA-CT·CdiI^{NC101}-His_6 complex was expressed in *E. coli* BL21(DE3)-Gold cells from plasmid pMCSG58-CPX200205. Cells were cultured in LB medium supplemented with 100 μg/ml ampicillin at 37°C for 6–8 h, then diluted 1:100 into 50 ml of M9 minimal 'pink' medium supplemented with 0.5% glycerol, 50 μg/ml ampicillin and trace minerals and vitamins (30). Cells were grown to an optical density at 600 nm (OD_{600}) of ∼0.8, and then the culture was cooled to 18°C. Seleno-methionine (SeMet) was added to a final concentration of 60 μg/ml along with L-isoleucine, L-leucine, L-lysine, L-phenylalanine, L-threonine and L-valine at 100 μg/ml. After 20 min, the culture was adjusted to 0.5 mM isopropyl-D-thiogalactopyranoside (IPTG) and incubated overnight. Cells were harvested by centrifugation, washed and resuspended in 50 mM Tris–HCl (pH 8.0), 500 mM NaCl, 10 mM 2-mercaptoethanol (2-ME), 10% glycerol. Cells were broken using Fast Break reagent (Promega), 10 μg/ml of lysozyme, 500 units of Benzonase Nuclease HC and Complete Protease Inhibitor Cocktail (Roche). Lysates were clarified by centrifugation and passage through a 0.22 μm filter, then loaded onto a Nickel

(II) Sepharose HisTrap column equilibrated in resuspension buffer. Proteins were eluted with a linear 20–250 mM gradient of imidazole in resuspension buffer. Fractions containing the CdiA-CT·CdiI^{NC101}-His$_6$ complex and co-purified EF-Tu were pooled and loaded onto a Hiload 26/60 Superdex 200 size-exclusion column equilibrated with 20 mM Tris–HCl (pH 7.5), 150 mM NaCl, 2 mM dithiothreitol. Fractions containing the ternary complex were pooled and concentrated to 15 mg/ml using an Amicon Ultracel 10K concentrator. Prior to crystallization, trypsin was added to the protein sample at a final concentration of 40 ng/μl, followed by incubation on ice for 4 h or overnight. Crystallization was performed at 4°C by sitting-drop vapor diffusion in 96-well Crystal Quick plates (Greiner Bio-one). Samples were digested for 4 h (EF-Tu^{tr}·CdiA-CT·CdiI^{NC101}), then crystallized in 0.05 M KCl, 0.1 M HEPES (pH 7.0), 1.0 M ammonium sulfate [optimized C2 conditions of Protein Complex Suite (Qiagen)]. The overnight digested complex (EF-Tu^{2,3}·CdiA-CT·CdiI^{NC101}) was crystallized in 0.1 M Tris–HCl (pH 8.0), 1.5 M ammonium sulfate. These crystals were used as microseeds for further screening, according to protocol from Douglas Instruments Ltd. with the Mosquito nanoliter liquid handler (TTP Labtech). Crystals formed in Hampton Research Index Screen under conditions containing 0.1 M NaCl, 0.1 M Bis-Tris (pH 6.5), 1.5 M ammonium sulfate.

Data collection, structure solution and refinement

Crystals were cryoprotected in their mother liquor supplemented with either 3.0 M ammonium sulfate (EF-Tu^{2,3}·CdiA-CT·CdiI^{NC101}, EF-Tu^{tr}·CdiA-CT·CdiI^{NC101}) or 28% sucrose (EF-Tu^{2,3}·CdiA-CT·CdiI^{NC101}) and flash-cooled in liquid nitrogen. Diffraction data were collected at the Structural Biology Center 19-ID beamline at the Advanced Photon Source, Argonne National Laboratory. Single-wavelength anomalous diffraction (SAD) datasets were collected at 100K near the selenium K-absorption edge and diffraction images processed with the HKL3000 suite (31). Intensities were converted to structure factor amplitudes in Ctruncate (32,33) from the CCP4 package (34). Refinement statistics show that the structures are of good quality as presented in Table 1 (35,36). The EF-Tu^{2,3}·CdiA-CT·CdiI^{NC101} structure was solved using the HKL3000 software pipeline (31) by the SAD method with Se peak data merged from the two crystals. Heavy atom positions were determined in SHELXD and initial phases were obtained from SHELXE (37). Initially, 10 Se atoms were identified. After their positions were refined, eight of these sites were used to calculate improved phases through iterations of MLPHARE (38) and DM (39). The initial model was built in Buccaneer (40), and the final model obtained through iterative manual rebuilding in COOT (41) and crystallographic refinement in Refmac (34,42) against the dataset obtained from the crystal cryoprotected in sucrose. The refinement protocol included optimization of translation/libration/screw (TLS) motion parameters with six, five and three groups defined for CdiA-CT^{NC101} (chain A), CdiI^{NC101} (chain B) and EF-Tu^{2,3} (chain C), respectively.

The EF-Tu^{tr}·CdiA-CT·CdiI^{NC101} structure was solved by two-step molecular replacement in Phaser-MR (43,44) with the EF-Tu^{2,3}·CdiA-CT·CdiI^{NC101} structure used as a template in the first step and truncated domain 1 of EF-Tu from the 1ERC model (residues 8–41, 68–204) used in a second step. Subsequently, the resulting initial model was morphed into the electron density with the Phenix morph module (44,45). The structure was completed by real-space modeling in COOT and crystallographic refinement in Refmac with TLS option (three groups for EF-Tu (chains CD and GH) and two groups for each toxin domain (chains A and E) and CdiI (chains B and F)). To automatically generated local NCS restraints, the EF-Tu^{2,3}·CdiA-CT·CdiI^{NC101} structure was used to generate external restraints by ProSMART (46). Refinement statistics are shown in Table 1. The atomic coordinates and structure factors have been deposited in the Protein Data Bank under accession codes 5I4Q (EF-Tu^{2,3}·CdiA-CT·CdiI^{NC101}) and 5I4R (EF-Tu^{tr}·CdiA-CT·CdiI^{NC101}).

Analysis of the initial anomalous map from two merged crystals of EF-Tu^{2,3}·CdiA-CT·CdiI^{NC101} and final anomalous map from a single crystal indicates that five of the identified heavy atom sites are contributed by toxin and immunity proteins. Two sites are totally incorrect and one represents a low occupancy Se atom from EF-Tu, with an anomalous signal detectable only in the two-crystal dataset. Thus, Met residues in CdiA-CT^{NC101} and CdiI^{NC101} have been modeled as SeMet, whereas native Met residues were modeled in EF-Tu, which did not appear to incorporate SeMet. Similarly, only the toxin and immunity proteins appeared to contain SeMet residues in the EF-Tu^{tr}·CdiA-CT·CdiI^{NC101} complex.

Protein purification for biochemical analyses

EF-Ts, EF-Tu and CdiA-CT·CdiI^{NC101} were over-produced as fusions to His$_6$-tagged thioredoxin, and tRNA nucleotidyltransferase (CCA-adding enzyme) carried a C-terminal His$_6$ epitope to facilitate purification. Cultures of *E. coli* CH2016 harboring expression plasmids were grown to $OD_{600} \sim 0.7$, and expression was induced with 1 mM IPTG. After incubation for 2 h, cells were harvested and frozen at −80°C. Cell pellets were re-suspended in lysis buffer [50 mM Tris–HCl (pH 7.5), 150 mM NaCl, 10 mM 2-ME, 0.05% Triton X-100, 20 mM imidazole] and broken by two passages through a French press at 20 000 psi. Cell debris was removed by two rounds of centrifugation at 16 000 ×*g* at 4°C. His$_6$-tagged proteins were purified by Ni^{2+}-affinity chromatography in lysis buffer. For the purification of CdiA-CT^{NC101} fusion protein, resins were washed with 20 mM Tris–HCl (pH 7.5), 6 M guanidine-HCl to denature and release CdiI^{NC101} prior to imidazole elution. His$_6$-tagged proteins were eluted with 20 mM Tris–HCl (pH 7.5), 250 mM imidazole and dialyzed against 20 mM sodium phosphate (pH 7.8), 150 mM NaCl, 10 mM 2-ME. Following dialysis, the purified fusion proteins were cleaved with His$_6$-tagged TEV protease, and the protease and His$_6$-TrxA fragment subsequently removed by Ni^{2+}-affinity chromatography. Purified proteins were quantified by absorbance at 280 nm using the following extinction coefficients: EF-Tu, 20 400 cm^{-1} M^{-1}; EF-Ts, 4470 cm^{-1} M^{-1};

Table 1. Data processing and refinement statistics

Processing Structure	EF-Tu^{2,3}·CdiA-CT·CdiI^{NC101}	EF-Tu^{tr}·CdiA-CT·CdiI^{NC101}
Wavelength (Å)	0.9793	0.9792
Resolution range (Å)[a]	30.00–2.35 (2.39–2.35)	30.00–3.30 (3.36–3.30)
Space group	$P42_12$	$P2_1$
Unit cell parameters (Å, °)	a = 131.16 c = 63.33	a = 74.40 b = 128.35 c = 100.36 β = 109.6
Unique reflections	23688 (1155)	26374 (1279)
Multiplicity	9.1 (7.3)	3.7 (3.7)
Completeness (%)	100 (100)	99.3 (98.2)
<I >/< σI>	20.0 (2.1)	10.6 (1.5)
Wilson B factor (Å^2)	37.2	63.3
R_{merge}[b]	0.125 (0.953)	0.118 (0.959)
CC1/2[c]	0.734	0.714
CC*[c]	0.920	0.913
Refinement		
Resolution (Å)	30.00–2.35	30.00–3.30
Reflections work/test set	22536/1125	24766/1008
R_{work}/R_{free}[d]	0.181/0.218	0.243/0.268
Average B factor (Å^2) (No of atoms)		
macromolecules	54.9 (3061)	116.5 (8885)
ligands	103.8 (6)	145.3 (56)
solvent	45.8 (92)	
Rmsd bond lengths (Å)	0.015	0.010
Rmsd bond angles (°)	1.633	1.45
Ramachandran favored[e] (%)	97.9	96.8
Ramachandran outliers (%)	0	0
Clashscore[e]	1.64	3.54

[a]Values in parentheses correspond to the highest resolution shell.
[b]$R_{merge} = \Sigma h \Sigma j |Ihj - <Ih>| / \Sigma h \Sigma j Ihj$, where Ihj is the intensity of observation j of reflection h.
[c]As defined by Karplus (35).
[d]$R = \Sigma h ||Fo| - |Fc|| / \Sigma h |Fo|$ for all reflections, where F_o and F_c are observed and calculated structure factors, respectively. R_{free} is calculated analogously for the test reflections, randomly selected and excluded from the refinement.
[e]As defined by Molprobity (36).

CdiA-CT^{NC101}, 29 340 cm^{-1} M^{-1}; CdiI^{NC101}, 28 420 cm^{-1} M^{-1}; and tRNA nucleotidyltransferase, 55 920 cm^{-1} M^{-1}.

In vivo toxin activity and competition co-cultures

Nuclease activity screens were performed by activating CdiA-CT toxins from *E. coli* isolates NC101, 3006 and 96.154 inside *E. coli* X90 cells. CdiI immunity proteins were tagged with a C-terminal ssrA(DAS) degron as described (47,48). Cells were grown in tetracycline-supplemented LB media for 1 h (OD_{600} ∼ 0.1), then *cdiA-CT*/*cdiI-DAS* expression was induced with 0.4% L-arabinose. Induced cultures were incubated at 37°C with shaking for 3 h, then harvested into an equal volume of ice-cold methanol. Cells were collected by centrifugation and frozen at −80°C for subsequent RNA extraction and analyses. This same approach was used to ascertain the toxicity of CdiA-CT^{NC101} domains harboring site-directed mutations. *E. coli* X90 cells carrying *cdiA-CT*/*cdiI-DAS* expression constructs were seeded at OD_{600} ∼ 0.05 in LB media supplemented with tetracycline and incubated with shaking at 37°C. After 60 min, the cultures were adjusted to 0.4% L-arabinose and cultured for an additional 4 h. Cell growth was monitored by measuring the OD_{600} of each culture every 30 min. Culture samples were harvested into an equal volume of ice-cold methanol after 2 h of induction and the cells frozen for subsequent RNA extraction.

Escherichia coli EPI100 inhibitor strains carrying cosmids pCH11434 (wild-type CdiA-CT^{NC101}), pCH12796 (Tyr192Arg), pCH13353 (Gln198Ala), pCH13354 (Arg200Ala), pCH13355 (Glu236Ala), pCH13356 (Gln250Ala) or pCH12749 (His248Ala) were co-cultured at a 1:1 ratio with rifampicin-resistant *E. coli* MC4100 target cells harboring the empty vector pTrc99A (*cdiI*$^-$) or pCH12042 (*cdiI*^{NC101}) in shaking LB media without antibiotics. Viable target cells were enumerated on selective media as colony forming units (cfu) per ml at the beginning of co-culture and after 2 h. The data from three independent experiments are reported together with the mean ± standard errors. For the analysis of toxic tRNase activity, samples were harvested into an equal volume of ice-cold methanol after 30 min of co-culture. Cells were collected by centrifugation and frozen at −80°C for subsequent RNA extraction.

RNA isolation and analyses

Frozen cell pellets were resuspended in guanidinium isothiocyanate (GITC)-phenol and total RNA extracted as described (49). RNAs (5 μg) were run on 8 M urea 10% polyacrylamide gels buffered with 0.5× Tris-borate ethylenediaminetetraacetic acid (EDTA) and electroblotted to positively charged nylon membranes for Northern blot analysis. Blots were hybridized with [^{32}P]-labeled oligonucleotide probes that are specific for individual *E. coli* tRNAs (see Supplementary Table S2) (49,50). Blots were visualized on a Bio-Rad phosphorimager using Quantity One software. S1 nuclease protection analysis was performed as described

(50) using oligonucleotide CH3916 to map the cleavage site at the 3′-end of $tRNA^{Glu}$. The S1 probe and marker oligonucleotides were first radiolabeled at their 3′-termini with [α-^{32}P]-cordycepin triphosphate and terminal transferase, then de-salted with a G-25 spin column and 5′-phosphorylated with T4 polynucleotide kinase and unlabeled adenosine triphosphate (ATP). Radiolabeled probe was hybridized with RNA samples for 4 h at 50°C, then digested with S1 nuclease at 37°C for 30 min. Reactions were quenched with sodium acetate (pH 5.0) and precipitated with 90% ethanol. Reaction samples were run on 50% urea/10% polyacrylamide gels buffered with 0.5× Tris-borate-EDTA and visualized by phosphorimaging. *In vitro* transcripts of $tRNA^{Asp}$ were prepared using phage T7 RNA polymerase as described (22). Oligonucleotide CH4013 was annealed to CH4014 to generate a template for full-length $tRNA^{Asp}$, and primers CH4013/CH4437 were annealed to generate the template for truncated $tRNA^{Asp}$ lacking the CCA nucleotide sequence. Each oligonucleotide cassette was end-filled with Klenow fragment to produce double-stranded transcription templates.

In vitro enzyme assays

In vitro nuclease assays were performed in reaction buffer [20 mM Tris–HCl (pH 7.5), 100 mM NaCl, 5 mM $MgCl_2$, 10 mM 2-ME, 1 mM GTP and 100 μg/μl bovine serum albumin]. Purified CdiA-CT^{NC101}, EF-Tu and/or EF-Ts were diluted to 1 μM in reaction buffer, and $CdiI^{NC101}$ was used at 3 μM. Protein mixtures were equilibrated for 30 min at room temperature. Reactions were then initiated by addition of *E. coli* total RNA to final concentration of 800 ng/μl, followed by incubation for 1 h at 37°C. Reactions were quenched with an equal volume of 25 sodium dodecyl sulphate-urea gel loading buffer and run on 50% urea, 7.5% polyacrylamide gels buffered with 0.5× Tris-borate-EDTA. Gels were electroblotted to nylon membranes for hybridization with radiolabeled oligonucleotide probes as described above. Toxin-digested RNA was purified by GITC–phenol extraction, then incubated with 2 μM tRNA nucleotidyltransferase in 50 mM Tris–HCl (pH 8.0), 5 mM $MgCl_2$, 10 mM 2-ME, 1 mM ATP, 1 mM CTP at 37°C for 30 min. Reactions were quenched with gel-loading buffer and analyzed by Northern blot. For GTPase activity assays, purified CdiA-CT^{NC101}, EF-Tu and EF-Ts were used at 0.5 μM final concentration and reactions were supplemented with 15 μM GTP/0.033 μM [α-^{32}P]-GTP. Reactions were initiated by the addition of *E. coli* total RNA to a final concentration of 0.9 μg/μl and incubated at ambient temperature for 10 min. Positive control reactions were conducted under the same conditions with oligonucleotide CH1737 (5 μM) and polynucleotide kinase. Reactions were resolved by thin-layer chromatography on polyethyleneimine cellulose (Polygram cel 300 PEI/UV254) using 0.3 M sodium phosphate (pH 3.5) as the mobile phase. Chromatograms were visualized by phosphorimaging.

Protein–protein binding was assessed by co-purification during Ni^{2+}-affinity chromatography. Proteins were mixed together at 5 μM final concentrations in binding buffer [20 mM Tris–HCl (pH 7.5), 150 mM NaCl, 20 mM imidazole, 5 mM $MgCl_2$, 1 mM GTP, 10 mM 2-ME, 0.05% Triton X-100] and incubated for 30 min at room temperature. Ni^{2+}-NTA agarose resin was added and incubated for 30 min at room temperature. Resins were washed with binding buffer, and column-bound proteins were eluted in binding buffer supplemented with 500 mM imidazole. Samples of the initial protein mixture, the unbound fraction and the eluted proteins were analyzed by sodium dodecyl sulphate-polyacrylamide gel electrophoresis and Coomassie blue staining.

RESULTS

Crystallization and structure determination

Isolation of the CdiA-CT·$CdiI^{NC101}$ complex by Ni^{2+}-affinity chromatography resulted in the co-purification of EF-Tu (Supplementary Figure S1A), suggesting that the toxin and immunity proteins form a stable ternary complex with this translation factor. EF-Tu is the most abundant cytosolic protein in *E. coli*, and is apparently present in sufficient quantity to form a stoichiometric complex with overproduced CdiA-CT·$CdiI^{NC101}$. To facilitate crystallization, the EF-Tu·CdiA-CT·$CdiI^{NC101}$ complex was subjected to limited proteolysis with trypsin. This treatment removed the N-terminal 'translocation' domain (Val1–Lys163) from CdiA-CT^{NC101} (28), leaving the ∼9.9 kDa C-terminal domain in the complex. Trypsin also cleaved EF-Tu at Arg45 and Arg59 to yield $EF\text{-}Tu^{tr}$, a previously characterized form that lacks the flexible switch I region (51–56). Upon prolonged digestion, the entire N-terminal GTPase domain was removed from EF-Tu to leave an ∼24 kDa fragment composed of β-barrel domains 2 and 3 ($EF\text{-}Tu^{2,3}$). $EF\text{-}Tu^{2,3}$·CdiA-CT·$CdiI^{NC101}$ crystallized in space group $P42_12$ with a single copy of the assembly in the asymmetric unit. The structure was solved by SAD phasing with Se-Met labeled protein to a resolution of 2.35 Å (Table 1 and Supplementary Figure S2A). The resulting model includes residues Gly168–Lys255 of CdiA-CT^{NC101}, Met1–Ala107 of $CdiI^{NC101}$ and Lys209–Gly394 of EF-Tu (Figure 1A). Crystal packing suggests that the ternary complex is a dimer of heterotrimer units related by a crystallographic two-fold axis. This is consistent with size-exclusion chromatography data showing that the mass of the complex is >158 kDa (Supplementary Figure S1B). $EF\text{-}Tu^{tr}$·CdiA-CT·$CdiI^{NC101}$ crystallized in space group $P2_1$ with two complexes per asymmetric unit, again indicating that the biological assembly is a dimer of heterotrimers. The latter structure was solved by molecular replacement using $EF\text{-}Tu^{2,3}$·CdiA-CT·$CdiI^{NC101}$ and domain 1 of EF-Tu as models and refined to a resolution of 3.30 Å (Table 1 and Supplementary Figure S2B). The final model includes all EF-Tu residues except Met1–Arg8 and Ala46–Arg59. $EF\text{-}Tu^{tr}$ adopts the GDP-bound conformation and two guanosine diphosphate molecules were identified in the structure (Figure 1B and Supplementary Figure S2C). Heterotrimeric assemblies from the two models superimpose with an average rmsd of 0.4 Å, with the toxin domains exhibiting the best fits and EF-Tu fragments showing the largest deviations between crystal forms (Supplementary Table S3). Because the structures are very similar, the following descriptions focus on the higher resolution $EF\text{-}Tu^{2,3}$·CdiA-CT·$CdiI^{NC101}$ model unless stated otherwise.

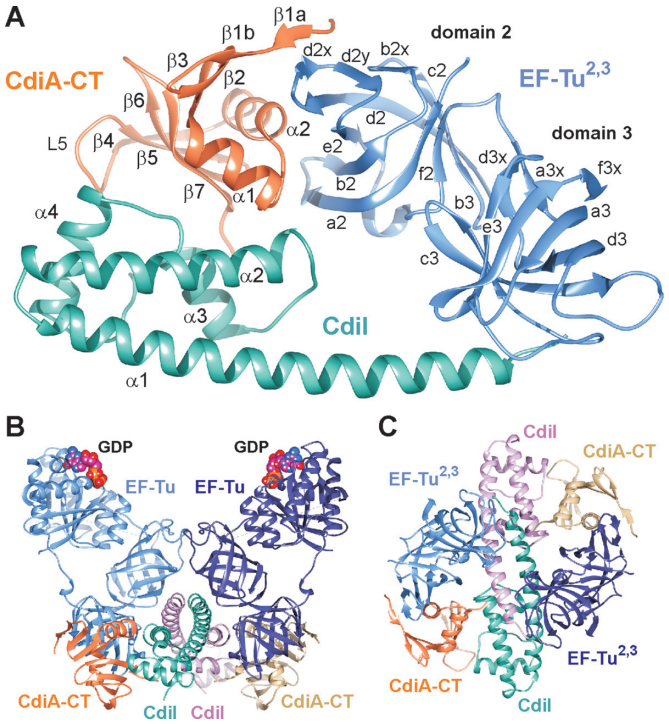

Figure 1. Structure of the EF-Tu·CdiA-CT·CdiI^{NC101} complex. (**A**) Monomeric EF-Tu^{2,3}·CdiA-CT·CdiI^{NC101} complex in a cartoon representation. EF-Tu secondary structure elements are indicated according to (60). (**B**) Dimeric EF-Tu^{tr}·CdiA-CT·CdiI^{NC101} complex in a cartoon representation. GDP molecules are depicted as spheres with carbon atoms colored pink. (**C**) The EF-Tu^{2,3}·CdiA-CT·CdiI^{NC101} dimer is rotated 90° with respect to panel B.

Structure of the CdiA-CT·CdiI^{NC101} complex

The C-terminal domain of CdiA-CT^{NC101} is globular with a central seven-stranded mixed β-sheet decorated by two α-helices (Figure 1A). Helix α1 caps the sheet and helix α2 runs parallel to its curvature. Extended loop L5 connects β4–β5 and forms a large pocket together with helix α1 on the C-terminal face of the toxin domain. DALI server searches revealed that the closest structural homologs of the toxin are BrnT from *Brucella abortus* ($Z = 7.1$) and the C-terminal tRNase domains of colicin D ($Z = 5.4$) and colicin E5 ($Z = 4.7$) (Supplementary Table S4 and Figure S3). The toxin domain is also similar to a number of mRNA interferases from *E. coli*, including MqsR ($Z = 4.5$), YoeB ($Z = 4.1$) and RelE ($Z = 3.3$). All of these homologs share the BECR superfamily fold (23).

The CdiI^{NC101} immunity protein consists of four α-helices that form an elongated club-like structure. Helices α2, α3 and α4 form a globular head from which the long N-terminal α1 helix protrudes (Figure 1A). CdiI^{NC101} mediates dimerization of the ternary complex through helices α1 and α2, which form a V-shaped structure that accepts the N-terminus of α1 from the adjacent immunity protomer (Figure 1B and C). The CdiI^{NC101} dimer interface buries ∼1300 Å^2, with a predicted interaction free energy of −22.4 kcal/mol as calculated by ePISA (57). The globular head of CdiI^{NC101} fits into the pocket on the C-terminal face of the toxin domain, burying ∼800 Å^2 of surface area ($\Delta G = -2.7$ kcal/mol). The toxin-immunity protein interaction is mediated primarily through a network of hydrogen-bonds (H-bonds) and salt bridges (Supplementary Table S5). CdiI^{NC101} residue Asp84 forms a salt bridge with toxin residue Arg200 and makes an additional direct contact with His248 (Figure 2A). The side-chain of CdiI^{NC101} Arg85 forms a prominent salt bridge with Asp220 from loop L5 of the toxin domain. Searches for structural homologs of CdiI^{NC101} identified BAG1 co-chaperones, a translin family nuclease from *Nanoarchaeum* and a human ADP-ribosylation factor binding protein (Supplementary Table S4). All of these structural homologs are monomeric and have functions that are unrelated to CdiI^{NC101}.

CdiA-CT/CdiI^{NC101} interactions with EF-Tu

In complex with CdiA-CT·CdiI^{NC101}, EF-Tu adopts the same overall conformation reported for the GDP-bound form (58–61), though the loops connecting strands a2 to b2 and d2 to e2 are displaced ∼6 Å and ∼9 Å (respectively) by the toxin domain (Figure 2B). The N-terminal face of the toxin interacts exclusively with EF-Tu domain 2 and buries ∼1000 Å^2 ($\Delta G = -13.9$ kcal/mol). CdiA-CT^{NC101} helix α2 packs onto the surface of the β-barrel, and strand β1a complements the exposed d2-d2x β-hairpin of EF-Tu to form an antiparallel three-stranded sheet (Figures 1A and 2C). The EF-Tu·CdiA-CT^{NC101} interface is coordinated by 13 H-bonds and ion-pairs (Supplementary Table S5). Lys171 within toxin strand β1a forms a salt bridge with EF-Tu residue Asp267, and toxin residue Tyr192 forms H-bonds with the side-chain of Glu260 and the main-chain amide of Arg263 in EF-Tu. The interface is further stabilized by hydrophobic interactions, including π–π stacking of the aromatic rings of toxin residue Trp196 and Phe262 of EF-Tu (Figure 2C).

Each EF-Tu molecule also interacts directly with both protomers of the CdiI^{NC101} dimer. Within the heterotrimeric assembly, helices α1 and α2 of CdiI^{NC101} engage EF-Tu domains 3 and 2, respectively (Figure 2D). These interactions are anchored by ion-pairs between Glu6 and Glu69 of the immunity protein and Arg328 and Arg284 of EF-Tu. Helix α1′ from the complementary immunity protomer occupies the groove between the EF-Tu β-barrel domains, and its intermolecular contacts are dominated by the guanidinium of Arg23, which interacts directly with Glu288, Thr336 and Asp337 of EF-Tu (Figure 2D and Supplementary Table S5). Stacking between CdiI^{NC101} Arg15 and EF-Tu Arg289 is also observed, in addition to a few weaker H-bonds and hydrophobic interactions. Overall, the two EF-Tu·CdiI^{NC101} interfaces total ∼630 Å^2.

CdiA-CT^{NC101} is a specific tRNase

The structural similarity between CdiA-CT^{NC101} and the BECR superfamily indicates that the toxin is likely a ribonuclease. The interaction with EF-Tu further suggests that tRNA is the preferred substrate. To identify substrates, we used controlled proteolysis to degrade CdiI^{NC101} carrying a C-terminal ssrA(DAS) degron, thereby activating the toxin *in vivo* as described previously (47,48). Northern blot analysis revealed that tRNA^{Asn}, tRNA^{Asp}, tRNA^{Glu},

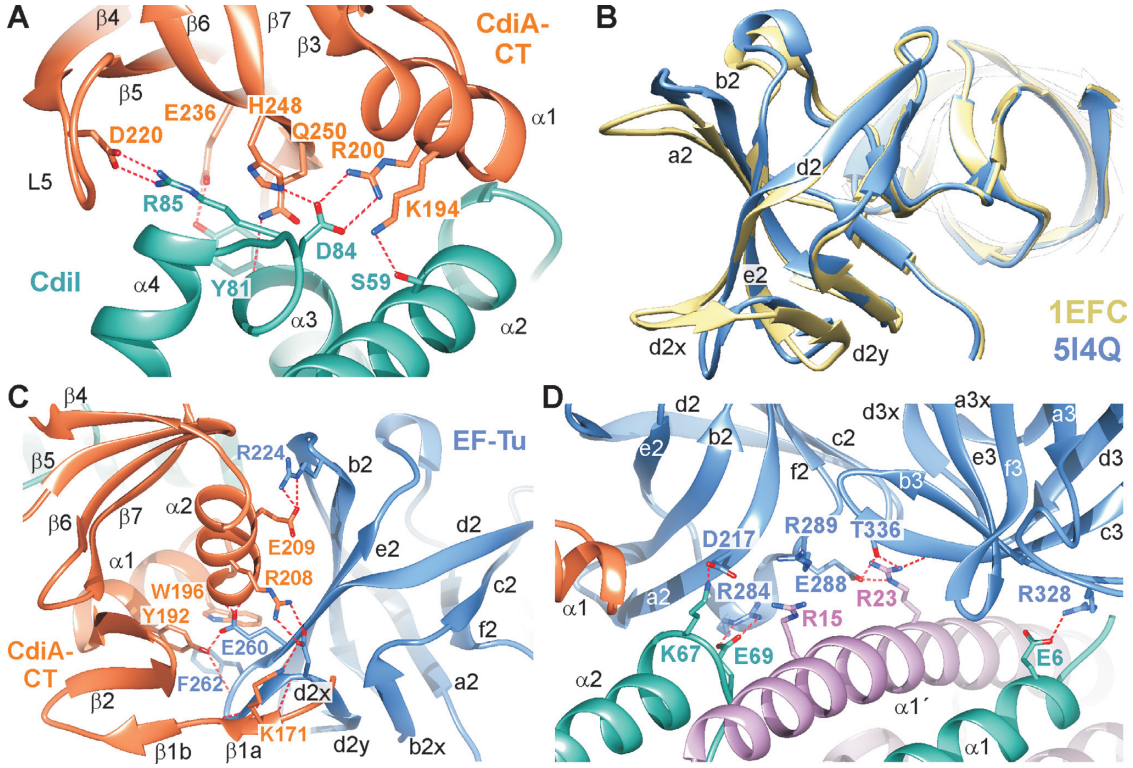

Figure 2. Intermolecular interactions. (**A**) The CdiA-CT·CdiI^{NC101} interface. (**B**) Superimposition of EF-Tu^{2,3} structures from free EF-Tu (PDB ID: 1EFC) and EF-Tu^{2,3}·CdiA-CT·CdiI^{NC101} (PDB ID: 5I4Q). (**C**) The EF-Tu·CdiA-CT^{NC101} interface. (**D**) Interactions between EF-Tu^{2,3} (blue) and the CdiI^{NC101} dimer (cyan and pink).

tRNA$_{UCU}^{Arg}$ and tRNA^{Ser} isoacceptors are cleaved in response to toxin activation (Figure 3A and Supplementary Figure S4). Limited activity was also observed on tRNA$_{CUG}^{Gln}$ and tRNA^{Trp} (Figure 3A and Supplementary Figure S4). We next tested whether these tRNA molecules are also cleaved in target bacteria during co-culture with inhibitor cells that deploy the CdiA-CT^{NC101} toxin. We mixed inhibitor and target bacteria at a 1:1 ratio in shaking broth for 1 h, then isolated total RNA from the mixed population for Northern blot analysis. Cleaved tRNAs were detected in co-cultures with non-immune target cells (Figure 3B). We note that only half of any given tRNA is cleaved in these samples, because inhibitor cells produce CdiI^{NC101}, which neutralizes toxin activity in this population (28). Accordingly, tRNA in target bacteria was protected from degradation when these cells expressed *cdiI*^{NC101} from a plasmid vector (Figure 3B). These results show that several tRNAs are efficiently cleaved in target bacteria, suggesting that these molecules are physiologically relevant substrates.

The slight increase in electrophoretic mobility observed for toxin-cleaved tRNA indicates that only a few nucleotides are removed. We used S1 nuclease protection to map the cleavage site on tRNA^{Glu} isolated from cells that were intoxicated by internal CdiA-CT^{NC101} expression (Figure 3A). This analysis revealed that four nucleotides are removed from the 3′-end, truncating the tRNA after nucleotide C72 (Figure 4B and C). The same cleavage site was observed in tRNA^{Glu} isolated from a competition co-culture with non-immune target bacteria (Figures 3B and 4B). We noted that preferred substrates all contain a guanine discriminator nucleotide adjacent to the cleavage site, suggesting this position is a specificity determinant. Therefore, we examined toxin activity on tRNA$_{UCU}^{Arg}$ and tRNA$_{CCU}^{Arg}$, which contain guanine and adenine discriminators, respectively (Figure 3C). We co-cultured inhibitor cells with target bacteria that over-produce each isoacceptor from a plasmid vector, then monitored tRNA degradation by Northern blot. Because tRNA$_{UCU}^{Arg}$ and tRNA$_{CCU}^{Arg}$ are not abundant in wild-type *E. coli* cells (62), the hybridization signal is dominated by the over-produced tRNA in the target cell population. tRNA$_{UCU}^{Arg}$ was completely cleaved after 1 h of co-culture, whereas tRNA$_{CCU}^{Arg}$ was unaffected (Figure 3C, lanes 2 and 4). We also probed these samples for tRNA^{Glu} to confirm that toxin was delivered into target bacteria during the co-culture (Figure 3C, lower blot). We then mutated the discriminator nucleotide in each isoacceptor to ascertain its importance in substrate recognition. The G74A substitution protected tRNA$_{UCU}^{Arg}$ from degradation, whereas tRNA$_{CCU}^{Arg}$ carrying the A72G mutation was efficiently cleaved (Figure 3C, lanes 3 and 5). Moreover, tRNA^{Tyr} was converted into a toxin substrate with a A82G discriminator mutation (Figure 3C, lanes 6 and 7). These results demonstrate that CdiA-CT^{NC101} possesses a highly specific nuclease activity that cleaves tRNA at the 5′-side of guanine discriminator nucleotides.

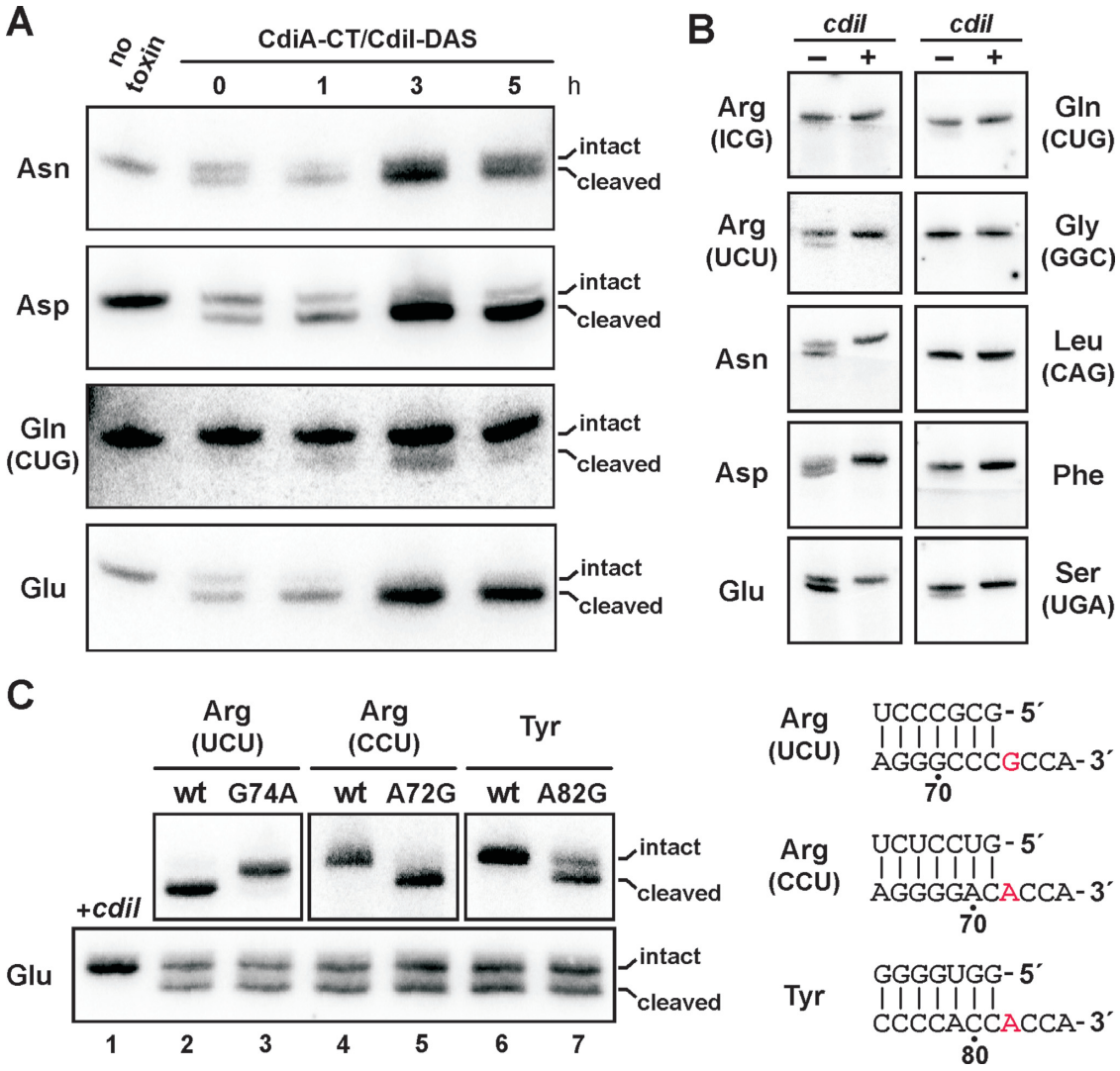

Figure 3. CdiA-CT^{NC101} is a specific tRNase. (**A**) CdiA-CT^{NC101} expression was induced in *Escherichia coli* and total RNA isolated at intervals for Northern blot analysis of the indicated tRNAs. (**B**) Inhibitor cells that deploy CdiA-CT^{NC101} were co-cultured at a 1:1 ratio with sensitive (*cdiI*$^{-}$) and immune (*cdiI*$^{+}$) target cells for 30 min, then total RNA was isolated for Northern blot analysis. Anticodon sequences are provided in parentheses to indicate specific tRNA isoacceptors. (**C**) Inhibitor cells that deploy CdiA-CT^{NC101} were co-cultured at a 1:1 ratio with target bacteria that over-express $tRNA_{UCU}^{Arg}$, $tRNA_{CCU}^{Arg}$ or $tRNA^{Tyr}$. Total RNA was then isolated for Northern blot analyses. $tRNA^{Glu}$ was monitored as a control to confirm toxin delivery into target cells. The sample in lane 1 (*cdiI*$^{+}$) was isolated from a co-culture containing target bacteria that express the *cdiI*^{NC101} immunity gene. Aminoacyl acceptor stems and discriminator nucleotides (in red) are presented on the right.

CdiA-CT^{NC101} nuclease active site

Superimposition of CdiA-CT^{NC101} onto BrnT suggests that the nuclease active site is located on the C-terminal face of the domain (Supplementary Figure S3). We reasoned that toxin residues Arg200, Glu236, His248 and Gln250 could participate directly in catalysis because their side-chains are clustered (Figure 2A), and they are completely conserved in homologous domains (Supplementary Figure S5). We also considered a role for Gln198, which is similarly positioned for catalysis and conserved in several related toxins (Supplementary Figure S5). We mutated each residue to Ala and examined *in vivo* activities using controlled proteolysis of degron-tagged CdiI^{NC101}. The His248Ala and Arg200Ala mutations abrogated growth inhibition activity, but the other mutations had no significant effect on toxicity (Figure 5A). Northern blot analysis confirmed that Arg200 and His248 are critical for nuclease activity, whereas the Gln198Ala, Glu236Ala and Gln250Ala mutations had no discernable effect on tRNA cleavage (Figure 5B). Similar results were obtained when the mutations were introduced into full-length CdiA and tested in CDI competition co-cultures. Cells that deploy the His248Ala and Arg200Ala domains failed to inhibit target bacteria, whereas the Gln198Ala and Gln250Ala toxins were as effective as wild-type toxin (Figure 5C). In contrast to its potent growth inhibition activity when expressed internally, we found that the Glu236Ala domain was attenuated when delivered into target cells during CDI (Figure 5C). To exclude the possibility that mutant CdiA function was abrogated by low expression or defective secretion, we examined the inactive effectors by immunoblot analysis using antibodies

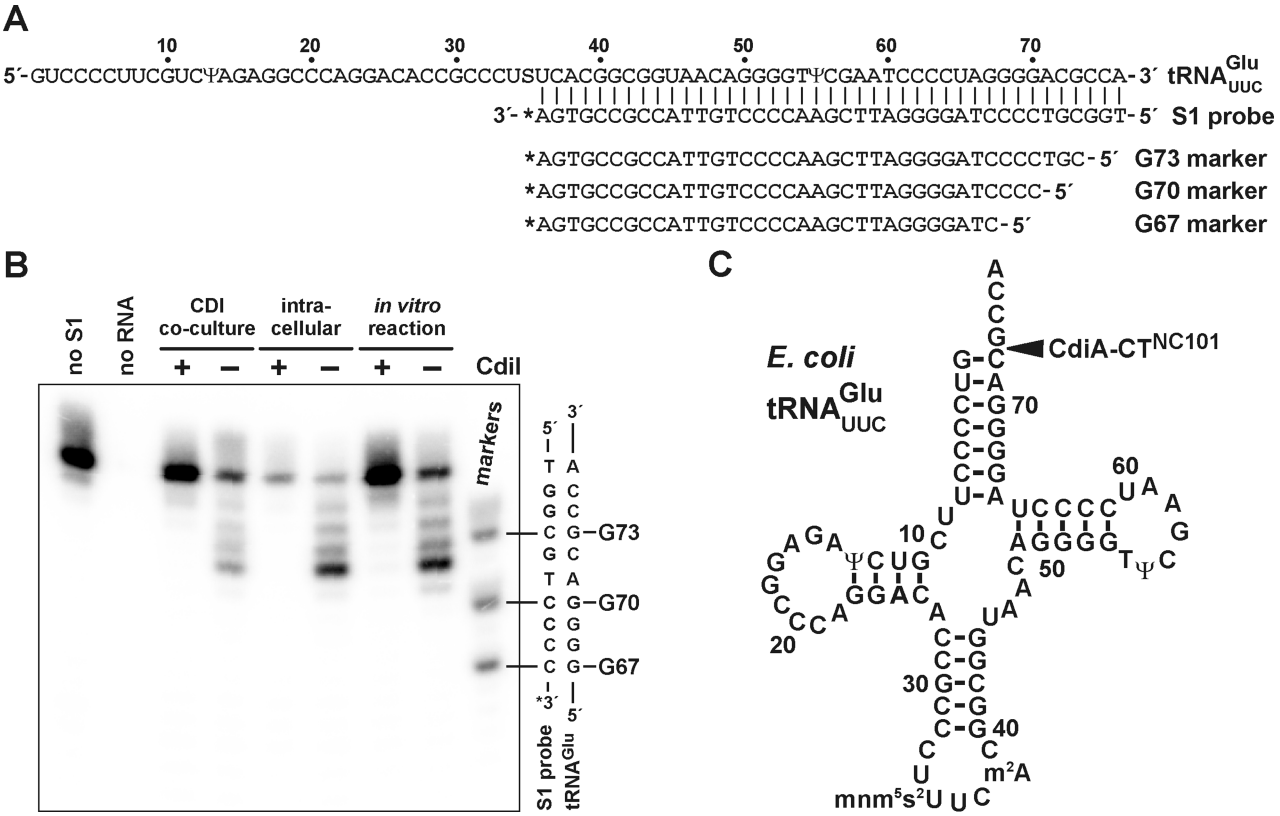

Figure 4. CdiA-CT^{NC101} cleaves the tRNA acceptor stem. (**A**) tRNA^{Glu} sequence showing the hybridized S1 probe and oligonucleotide standards used to map the toxin cleavage site. (**B**) S1 nuclease protection assays. RNA was isolated from competition co-cultures and cells intoxicated by intracellular CdiA-CT^{NC101} expression. Samples from *in vitro* tRNase reactions were also analyzed. Where indicated, the neutralizing effect of CdiI^{NC101} immunity protein was examined. RNA samples were incubated with the 3′-radiolabeled S1 probe and treated with S1 nuclease as described in 'Materials and Methods' section. A portion of the S1 probe-tRNA^{Glu} heteroduplex sequence is shown to the right of the autoradiogram. (**C**) The arrow indicates cleavage site within the acceptor stem of tRNA^{Glu}.

against the N-terminal domain of CdiA (63). This analysis showed that each CdiA variant accumulated to approximately the same level as wild-type (Supplementary Figure S6). Moreover, treatment with extracellular proteinase K revealed that each CdiA protein was exported to the cell surface (Supplementary Figure S6). Taken together, these results indicate that Arg200 and His248 are critical for tRNase activity and that Glu236 significantly contributes to toxicity in the context of cell-mediated CDI.

CdiA-CT^{NC101} tRNase activity is dependent on EF-Tu and EF-Ts

Because CdiA-CT^{NC101} binds to EF-Tu and has tRNase activity, we reasoned that the toxin probably requires EF-Tu to cleave substrate. Consistent with this hypothesis, CdiA-CT^{NC101} has no detectable nuclease activity in defined reactions containing purified toxin and total RNA isolated from *E. coli* (Figure 6A, lane 2). However, inclusion of purified EF-Tu failed to stimulate tRNase activity (Figure 6A, lane 3). We previously reported that mutations in the coiled-coil domain of elongation factor Ts (EF-Ts) provide resistance to CdiA-CT^{NC101} toxin (22), suggesting that EF-Ts may also be required for nuclease activity. Reactions supplemented with both EF-Tu and EF-Ts supported efficient cleavage of tRNA^{Glu} *in vitro* (Figure 6A, lane 5). This activity was neutralized with purified CdiI^{NC101} immunity protein (Figure 6A, lane 6), indicating that the reaction is catalyzed by CdiA-CT^{NC101} rather than contaminating nucleases in the various protein preparations. Moreover, this activity was indistinguishable from that detected *in vivo*, with tRNA^{Glu} cleaved after residue C72 (Figure 4B). We note that S1 nuclease protection also showed intermediate cleavage products, suggesting that CdiA-CT^{NC101} may act as an exonuclease to progressively remove residues from the 3′-end of the substrate. However, all tRNA molecules carry the same 3′ CCA sequence, so it is unclear why only a subset is cleaved *in vivo* (Supplementary Figure S4). One possibility is that the toxin cleaves CCA non-specifically, but cannot remove the discriminator nucleotide from non-preferred substrates. In this model, tRNA nucleotidyltransferase would rapidly repair damaged molecules that retain the discriminator nucleotide, which is required for CCA-addition (64). We explored this model by first asking whether other substrates are degraded *in vitro*, where nucleotidyltransferase is not available for repair. We treated *E. coli* total RNA with purified toxin, EF-Tu and EF-Ts and analyzed several tRNAs by Northern blot. tRNA^{Asp} and tRNA^{Glu} were cleaved efficiently under these conditions, but none of the other tRNAs were degraded (Figure 6B). Moreover, tRNA nucleotidyltransferase was unable to repair toxin-cleaved

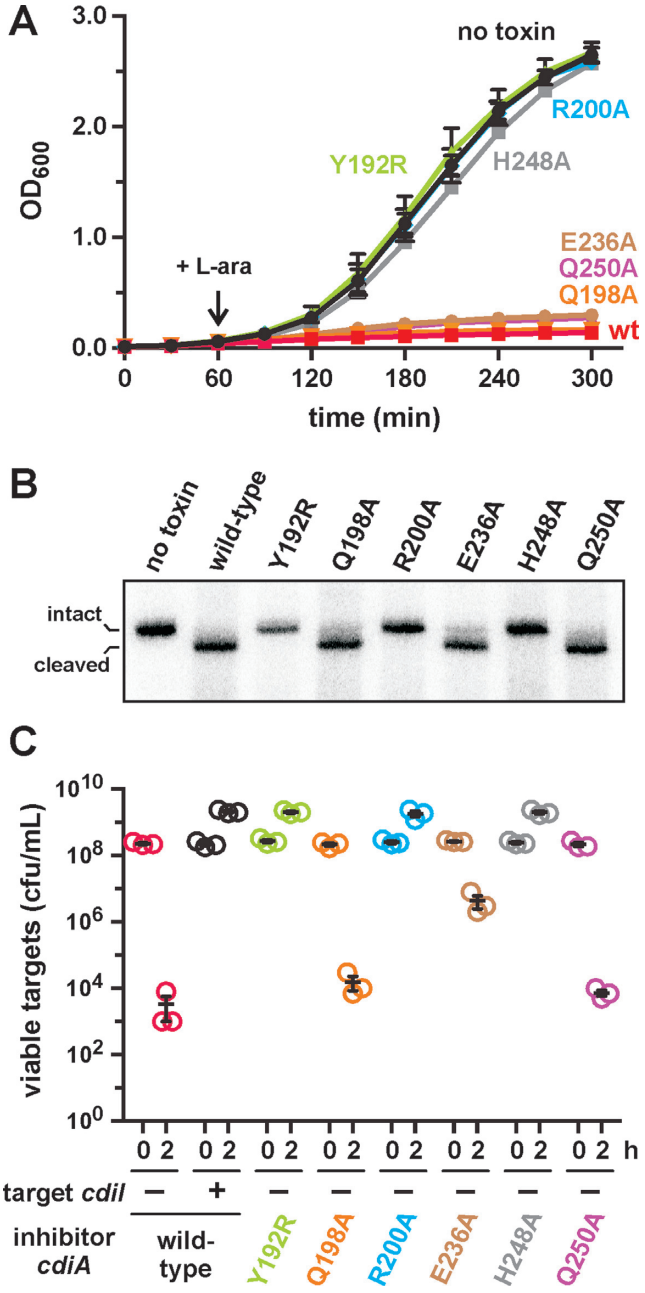

Figure 5. Mutagenesis of the CdiA-CT^{NC101} active site. (**A**) Expression of the indicated toxin variants was induced at 60 min with L-arabinose, and cell growth was monitored by measuring the optical density of the cultures at 600 nm (OD_{600}). (**B**) Northern blot analysis of RNA isolated at 180 min from the cultures in panel A. (**C**) Target bacteria were co-cultured at a 1:1 ratio with inhibitor cells that deliver the indicated CdiA-CT^{NC101} toxin variants. Where indicated (+), target cells carried a plasmid-borne copy of the *cdiI*^{NC101} immunity gene. Viable target cells were quantified as colony forming units per ml at 0 and 2 h. Data from three independent experiments and the bars indicate the standard error of the mean.

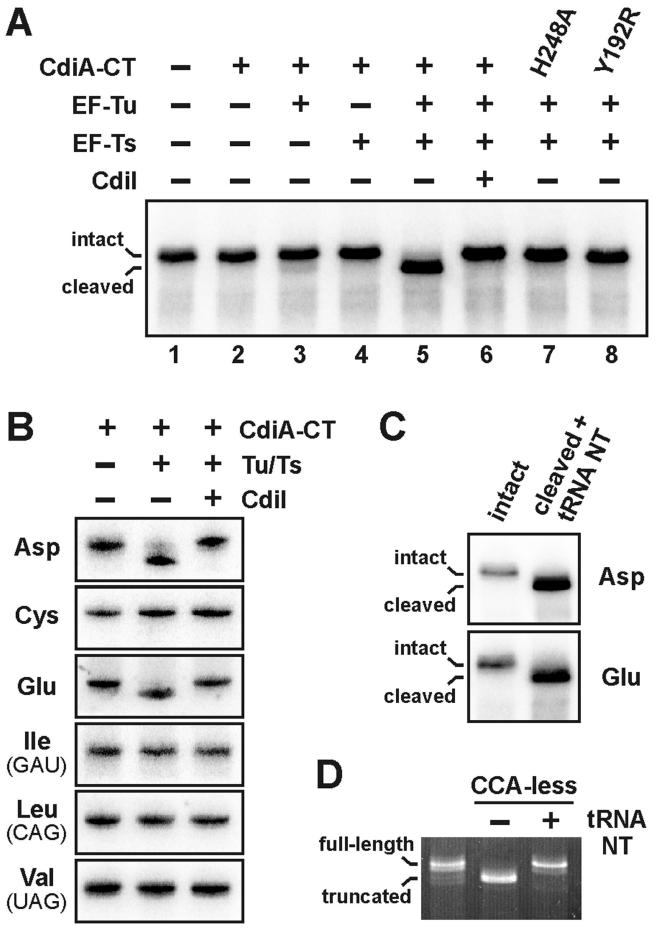

Figure 6. *In vitro* tRNase and GTPase assays. (**A**) Purified CdiA-CT^{NC101}, EF-Tu, EF-Ts and CdiI^{NC101} were incubated in GTP-supplemented buffer for 15 min. Total *Escherichia coli* RNA was then added and the solutions incubated at 37°C for 1 h. Reactions were analyzed by Northern blot for tRNA^{Glu}. (**B**) *In vitro* nuclease reactions were conducted as in panel A and reactions analyzed by Northern blot for the indicated tRNA species. Anticodon sequences are provided in parentheses to indicate specific isoacceptors. (**C**) RNA was isolated from *in vitro* nuclease reactions, then treated with tRNA nucleotidyltransferase (tRNA NT) in ATP/CTP supplemented buffer for 1 h at 37°C. Reactions were analyzed by Northern blot with probes for tRNA^{Asp} and tRNA^{Glu}. (**D**) tRNA nucleotidyltransferase is active on truncated tRNA that retains the discriminator nucleotide. tRNA^{Asp} truncated at residue G74 was prepared by *in vitro* transcription and incubated with tRNA nucleotidyltransferase (tRNA NT) as in panel C. The reaction was run on a denaturing polyacrylamide gel and visualized by ethidium bromide staining. Full-length tRNA^{Asp} transcript was run in the left lane for comparison.

tRNA^{Asp} and tRNA^{Glu} (Figure 6C), though it readily extended truncated tRNA^{Asp} transcripts that retain the discriminator nucleotide (Figure 6D). Together, these results suggest that CdiA-CT^{NC101} is an endonuclease that cleaves the single-stranded 3′-tail from specific tRNAs. Thus, the additional products observed in Figure 4B probably reflect incomplete S1 digestion of the tRNA:probe heteroduplex, rather than toxin degradation intermediates.

The finding that EF-Ts promotes tRNase activity raises the possibility that CdiA-CT^{NC101} forms a ternary complex with EF-Tu and EF-Ts. However, we did not detect EF-Ts·EF-Tu·CdiA-CT^{NC101} complexes by Ni^{2+}-affinity chromatography in the presence of either GDP or GTP (Supplementary Figure S7A). Surprisingly, we also did not observe a binary EF-Tu·CdiA-CT^{NC101} complex in these latter experiments (Supplementary Figure S7A). However, when purified CdiI^{NC101} was included in the protein mixture, we isolated stable EF-Tu·CdiA-CT·CdiI^{NC101} ternary

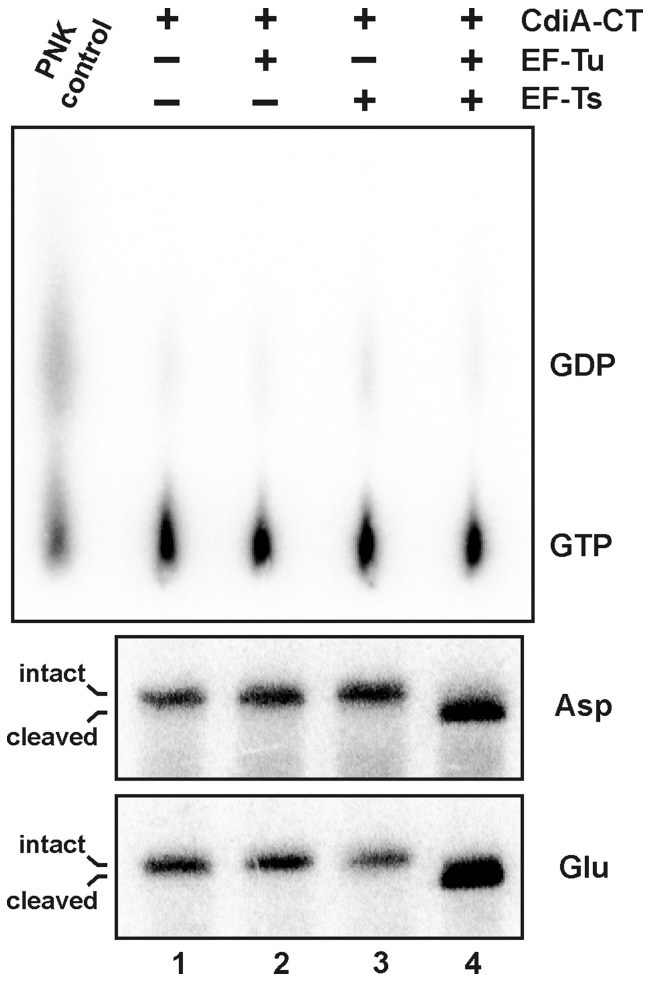

Figure 7. GTPase assays. tRNase reactions were conducted as described in Figure 6, but the buffer was supplemented with radiolabeled [α-^{32}P]-GTP. A polynucleotide kinase (PNK) reaction using [α-^{32}P]-GTP as the phosphoryl donor was included as a positive control. Reactions were analyzed by thin-layer chromatography (upper panel) and Northern blot hybridization (lower panels). The migration positions of GDP and GTP are indicated.

complexes (Supplementary Figure S7B). Thus, the toxin has lower affinity for EF-Tu in the absence of its immunity protein, suggesting that the EF-Tu·CdiI^{NC101} interfaces contribute significantly to complex stability. We also considered the possibility that EF-Ts promotes toxin activity in its capacity as a guanine nucleotide exchange factor (GEF) for EF-Tu. In this model, the toxin induces EF-Tu GTPase activity, and EF-Ts accelerates the nuclease reaction by reloading EF-Tu with GTP for additional turnover events. Therefore, we tested whether GTPase activity is stimulated during the tRNase reaction. We supplemented *in vitro* nuclease reactions with radiolabeled [α-^{32}P]-GTP and followed its conversion into [α-^{32}P]-GDP using thin-layer chromatography. However, we did not detect an increase in GDP production under conditions that support efficient tRNase activity (Figure 7, compare lane 4 to lanes 1–3). These data indicate that the role of EF-Ts in toxin-catalyzed tRNA cleavage does not require its intrinsic GEF activity.

Though the isolated toxin domain has relatively low affinity for EF-Tu (Supplementary Figure S7A), *in vitro* assays indicate that the translation factor is clearly required for nuclease activity. To confirm this requirement, we introduced a Tyr192Arg mutation into the toxin to disrupt its EF-Tu-binding interface (Figure 2C). The resulting domain retained its affinity for His$_6$-tagged CdiI^{NC101}, which facilitated purification of this toxin variant. However, EF-Tu no longer co-purified with the Tyr192Arg toxin-immunity protein complex (data not shown). Furthermore, the EF-Tu·CdiA-CT·CdiI^{NC101} ternary complex could not be reconstituted from purified constituents with the Tyr192Arg toxin domain (Supplementary Figure S7C), demonstrating that the mutation disrupts the interaction with EF-Tu. The purified Tyr192Arg toxin showed no detectable tRNase activity in reactions supplemented with both EF-Tu and EF-Ts, similar to the inactive domain carrying the His248Ala mutation (Figure 6A, lanes 7 and 8). The Tyr192Arg variant also lacked tRNase activity when expressed inside *E. coli* (Figure 5A and B), and did not inhibit target bacteria in CDI competition co-cultures (Figure 5C). Collectively, these results demonstrate that EF-Tu is required for CdiA-CT^{NC101} tRNase activity.

DISCUSSION

The CdiA^{NC101} effector carries an RNase domain that interacts with EF-Tu and cleaves the 3′-ends of specific tRNAs. Given that EF-Tu is required for *in vitro* tRNase activity, these findings suggest that substrate is cleaved only in the context of GTP·EF-Tu·aa-tRNA ternary complexes. In this model, the binding site on EF-Tu provides access to the tRNA acceptor stem. The 3′-end of aa-tRNA binds in the cleft between domains 1 and 2 of EF-Tu (59,60), and superimposition of the toxin onto GTP·EF-Tu·aa-tRNA shows that the nuclease active site is directed toward the acceptor stem (Figure 8A). However, the putative active-site imidazole of His248 is predicted to be ∼16 Å from the 2′-hydroxyl of C72 and ∼12 Å from the scissile phosphodiester bond. Further, the superimposition reveals several intermolecular clashes. Toxin helix α1 interferes with the switch I region in EF-Tu domain 1 (Figure 8B), and the N-terminus of EF-Tu clashes with the inter-molecular β-sheet (Figure 8C). The loop connecting toxin helices α1 and α2 clashes with the 3′-end of aa-tRNA (Figure 8C), and displacement of the d2-d2x β-hairpin should break the ion-pair linking Arg263 of EF-Tu to the 5′-phosphate of the terminal adenosine ribonucleotide (Figure 8D). Thus, the nuclease domain is predicted to disrupt contacts between the 3′-end of aa-tRNA and EF-Tu. Moreover, the clash with switch I suggests that the toxin could induce conformational changes in EF-Tu similar to those that occur during decoding on the ribosome. The β-turn connecting a2 and b2 of EF-Tu is relocated upon codon-anticodon recognition, distorting the interaction between the 3′-end of aa-tRNA and switch I to induce GTP hydrolysis (65,66). Following hydrolysis, domain 1 rotates ∼100° relative to domains 2/3, and EF-Tu adopts an extended conformation with low affinity for aa-tRNA (58,67). Toxin-induced rearrangement of the a2-b2 β-turn is more pronounced than that observed for ribosome-bound EF-Tu, yet the nuclease domain does not stimulate GTP hy-

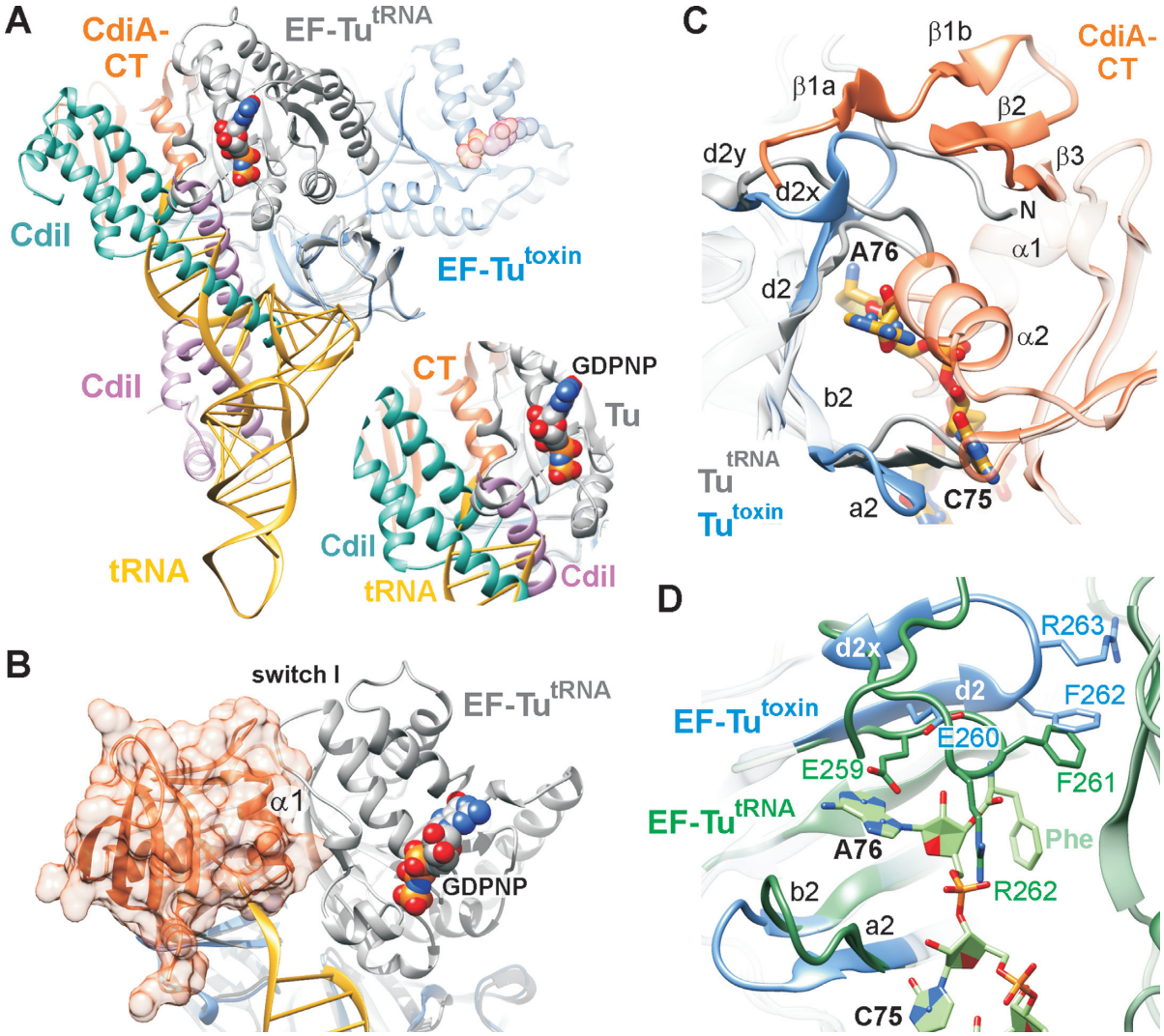

Figure 8. CdiA-CT^{NC101} disrupts contacts between EF-Tu and aa-tRNA. (**A**) Superposition of GDP·EF-Tu^{tr}·CdiA-CT·CdiI^{NC101} onto the GDPNP·EF-Tu·aa-tRNA ternary complex from *Thermus aquaticus* (PDB ID: 1B23). For clarity, only CdiI^{NC101} is shown as a dimer. The expanded region shows CdiA-CT^{NC101} clashing with domain 1 of EF-Tu and tRNA. Guanine nucleotides are shown as spheres. (**B**) Potential clashes between CdiA-CT^{NC101} helix α1 and the switch I region of EF-Tu. (**C**) Superimposition of EF-Tu in tRNA-bound (Tu^{tRNA}) and toxin-bound (Tu^{toxin}) states. The predicted clash between CdiA-CT^{NC101} helix α2 and residues C75 and A76 at the 3′-end of tRNA is illustrated. (**D**) Rearrangement of the aa-tRNA binding site. EF-Tu from the EF-Tu^{2,3}·CdiA-CT·CdiI^{NC101} structure is superimposed on the kirromycin-stabilized GTP·EF-Tu·aa-tRNA complex from *Escherichia coli* (PDB ID: 1OB2). The unnumbered Phe is the 3′-aminoacylated residue. EF-Tu numbering differs because 1OB2 does not include the initiating Met residue.

drolysis. Together, these observations suggest that the toxin remodels GTP·EF-Tu·aa-tRNA complexes to disrupt interactions between the translation factor and the 3′-end of aa-tRNA. Once liberated from its contacts with EF-Tu, the single-stranded tail of substrate tRNA is presumably free to enter the nuclease active site.

The CDI toxin deployed by *E. coli* strain EC869 also cleaves tRNA in an EF-Tu-dependent manner (22), but CdiA-CT^{NC101} and CdiA-CT^{EC869} differ in several respects. First, the nucleases share no sequence similarity, though given the lack of homology between known BECR toxins and CdiA-CT^{NC101}, the CdiA-CT^{EC869} domain could still adopt the same fold. Second, the two toxins have distinct substrate specificities, with CdiA-CT^{EC869} cleaving tRNA^{Gln} and tRNA^{Asn} at a different position within the acceptor-stem duplex. Third, CdiA-CT^{EC869} binds EF-Tu with high affinity even in the absence of its cognate immunity protein (22). Finally, the two CDI toxins appear to have different requirements for EF-Ts. EF-Ts stimulates CdiA-CT^{EC869} activity, but is not absolutely required for tRNA cleavage (22). By contrast, CdiA-CT^{NC101} activity is not detected *in vitro* unless both EF-Ts and EF-Tu are present. Despite this discrepancy, we propose that EF-Ts stimulates the activity of each toxin by increasing steady-state GTP·EF-Tu·aa-tRNA substrate levels as described by Blanchard and colleagues (68,69). Though EF-Tu has nanomolar affinity for aa-tRNA at 0–4°C (70), these interactions are estimated to be 20- to 30-fold weaker at 37°C (71,72), indicating that the dissociation constants approach the micromolar range under the conditions used here to monitor *in vitro* tRNase activity. Coupled with the low affinity of CdiA-CT^{NC101} for EF-Tu, *in vitro* nuclease activity is presumably impeded

by the low probability that EF-Tu, aa-tRNA and toxin all converge simultaneously. By contrast, the dynamic nature of EF-Tu·aa-tRNA binding has less of an effect on CdiA-CT^{EC869} tRNase activity, because this toxin forms a stable, high-affinity binary complex with EF-Tu (22). We note that CdiA-CT^{NC101} remains a potent nuclease *in vivo*, because cytoplasmic EF-Tu is present at sufficiently high concentrations (50–60 μM) (73) to drive toxin-binding through mass action. Thus, although relatively few toxin domains are delivered into target cells during CDI (74), the natural abundance of substrate presumably relieves the selective pressure for CdiA-CT^{NC101} to evolve high-affinity interactions with EF-Tu.

The CdiA-CT^{NC101} nuclease domain shares the BECR fold and most closely resembles BrnT and the C-terminal tRNase domain of colicin D. Surprisingly, recent computational surveys of prokaryotic toxin domains did not uncover CdiA-CT^{NC101} (nor any of its homologs) as members of the BECR superfamily (23,75). Structural homology is often presumed to indicate a common evolutionary history; but the colicin D immunity protein does not share any sequence or structural similarity with CdiI^{NC101}, suggesting that the corresponding nuclease domains are related through convergent evolution. Further, the structural similarities with RelE and YoeB are intriguing, because these toxins also require a macromolecular scaffold for substrate recognition, cleaving mRNA only when presented in the ribosome A site (76,77). The advantage of scaffold-dependent activity is not immediately apparent. Scaffolds are not necessary for these types of reactions, because several type II toxins degrade mRNA in a ribosome-independent manner (78,79), and other CDI toxins are known to cleave tRNA acceptor stems in the absence of EF-Tu (16,28). Perhaps scaffold-dependent activity is merely an inevitable consequence of toxin evolution in the densely packed bacterial cytoplasm, where EF-Tu and ribosomes are abundant. However, scaffolds provide additional substrate specificity, and therefore should restrict the activity of potential lethal nucleases. This property may be advantageous for type II toxin-antitoxin systems, which are hypothesized to mediate reversible growth stasis and persistence (80,81). Such safe-guards could also protect CDI$^+$ bacteria in the event that their immunity protein levels decrease transiently. Alternatively, it is possible that interactions between CDI toxins and EF-Tu serve other physiological functions. In this model, neutralized EF-Tu·CdiA-CT·CdiI complexes could influence gene expression, and thereby mediate cell-to-cell signaling between siblings as proposed recently for *Burkholderia thailandensis* (82). We note that CDI toxins from *E. coli* 96.154 and *Klebsiella pneumoniae* 342 also interact with EF-Tu, suggesting that this phenomenon may be quite common. It is unclear whether these sequence-diverse toxin domains bind EF-Tu in the same manner, and the consequences of this widespread phenomenon on bacterial physiology remain to be explored.

ACCESSION NUMBERS

PDB IDs: 5I4Q and 5I4R.

SUPPLEMENTARY DATA

Supplementary Data are available at NAR Online.

FUNDING

National Institutes of Health (NIH) [GM094585, GM115586 to A.J., GM117373 to C.W.G., D.A.L., C.S.H.]; U. S. Department of Energy, Office of Biological and Environmental Research [DE-AC02-06CH11357 to A.J.]. Funding for open access charge: NIH grant [GM117373].
Conflict of interest statement. None declared.

REFERENCES

1. Waksman,S. (1961) The role of antibiotics in nature. *Perspect. Biol. Med.*, **4**, 271–286.
2. Cascales,E., Buchanan,S.K., Duche,D., Kleanthous,C., Lloubes,R., Postle,K., Riley,M., Slatin,S. and Cavard,D. (2007) Colicin biology. *Microbiol. Mol. Biol. Rev.*, **71**, 158–229.
3. Aoki,S.K., Pamma,R., Hernday,A.D., Bickham,J.E., Braaten,B.A. and Low,D.A. (2005) Contact-dependent inhibition of growth in *Escherichia coli*. *Science*, **309**, 1245–1248.
4. Hood,R.D., Singh,P., Hsu,F., Guvener,T., Carl,M.A., Trinidad,R.R., Silverman,J.M., Ohlson,B.B., Hicks,K.G., Plemel,R.L. *et al.* (2010) A type VI secretion system of *Pseudomonas aeruginosa* targets a toxin to bacteria. *Cell Host Microbe*, **7**, 25–37.
5. Souza,D.P., Oka,G.U., Alvarez-Martinez,C.E., Bisson-Filho,A.W., Dunger,G., Hobeika,L., Cavalcante,N.S., Alegria,M.C., Barbosa,L.R., Salinas,R.K. *et al.* (2015) Bacterial killing via a type IV secretion system. *Nat. Commun.*, **6**, 6453.
6. Whitney,J.C., Peterson,S.B., Kim,J., Pazos,M., Verster,A.J., Radey,M.C., Kulasekara,H.D., Ching,M.Q., Bullen,N.P., Bryant,D. *et al.* (2017) A broadly distributed toxin family mediates contact-dependent antagonism between gram-positive bacteria. *Elife*, **6**, e26938.
7. Aoki,S.K., Malinverni,J.C., Jacoby,K., Thomas,B., Pamma,R., Trinh,B.N., Remers,S., Webb,J., Braaten,B.A., Silhavy,T.J. *et al.* (2008) Contact-dependent growth inhibition requires the essential outer membrane protein BamA (YaeT) as the receptor and the inner membrane transport protein AcrB. *Mol. Microbiol.*, **70**, 323–340.
8. Aoki,S.K., Webb,J.S., Braaten,B.A. and Low,D.A. (2009) Contact-dependent growth inhibition causes reversible metabolic downregulation in *Escherichia coli*. *J. Bacteriol.*, **191**, 1777–1786.
9. Aoki,S.K., Diner,E.J., de Roodenbeke,C.T., Burgess,B.R., Poole,S.J., Braaten,B.A., Jones,A.M., Webb,J.S., Hayes,C.S., Cotter,P.A. *et al.* (2010) A widespread family of polymorphic contact-dependent toxin delivery systems in bacteria. *Nature*, **468**, 439–442.
10. Nikolakakis,K., Amber,S., Wilbur,J.S., Diner,E.J., Aoki,S.K., Poole,S.J., Tuanyok,A., Keim,P.S., Peacock,S., Hayes,C.S. *et al.* (2012) The toxin/immunity network of *Burkholderia pseudomallei* contact-dependent growth inhibition (CDI) systems. *Mol. Microbiol.*, **84**, 516–529.
11. Anderson,M.S., Garcia,E.C. and Cotter,P.A. (2012) The *Burkholderia bcpAIOB* genes define unique classes of two-partner secretion and contact dependent growth inhibition systems. *PLoS Genet.*, **8**, e1002877.
12. Arenas,J., Schipper,K., van Ulsen,P., van der Ende,A. and Tommassen,J. (2013) Domain exchange at the 3′ end of the gene encoding the fratricide meningococcal two-partner secretion protein A. *BMC Genomics*, **14**, 622.
13. Mercy,C., Ize,B., Salcedo,S.P., de Bentzmann,S. and Bigot,S. (2016) Functional characterization of *Pseudomonas* contact dependent growth inhibition (CDI) systems. *PLoS One*, **11**, e0147435.
14. Ruhe,Z.C., Low,D.A. and Hayes,C.S. (2013) Bacterial contact-dependent growth inhibition. *Trends Microbiol.*, **21**, 230–237.
15. Willett,J.L., Ruhe,Z.C., Goulding,C.W., Low,D.A. and Hayes,C.S. (2015) Contact-dependent growth inhibition (CDI) and CdiB/CdiA two-partner secretion proteins. *J. Mol. Biol.*, **427**, 3754–3765.
16. Morse,R.P., Nikolakakis,K.C., Willett,J.L., Gerrick,E., Low,D.A., Hayes,C.S. and Goulding,C.W. (2012) Structural basis of toxicity and

immunity in contact-dependent growth inhibition (CDI) systems. *Proc. Natl. Acad. Sci. U.S.A.*, **109**, 21480–21485.
17. Beck,C.M., Morse,R.P., Cunningham,D.A., Iniguez,A., Low,D.A., Goulding,C.W. and Hayes,C.S. (2014) CdiA from *Enterobacter cloacae* delivers a toxic ribosomal RNase into target bacteria. *Structure*, **22**, 707–718.
18. Morse,R.P., Willett,J.L., Johnson,P.M., Zheng,J., Credali,A., Iniguez,A., Nowick,J.S., Hayes,C.S. and Goulding,C.W. (2015) Diversification of beta-Augmentation Interactions between CDI Toxin/Immunity Proteins. *J. Mol. Biol.*, **427**, 3766–3784.
19. Johnson,P.M., Beck,C.M., Morse,R.P., Garza-Sanchez,F., Low,D.A., Hayes,C.S. and Goulding,C.W. (2016) Unraveling the essential role of CysK in CDI toxin activation. *Proc. Natl. Acad. Sci. U.S.A.*, **113**, 9792–9797.
20. Johnson,P.M., Gucinski,G.C., Garza-Sanchez,F., Wong,T., Hung,L.W., Hayes,C.S. and Goulding,C.W. (2016) Functional diversity of cytotoxic tRNase/immunity protein complexes from *Burkholderia pseudomallei*. *J. Biol. Chem.*, **291**, 19387–19400.
21. Diner,E.J., Beck,C.M., Webb,J.S., Low,D.A. and Hayes,C.S. (2012) Identification of a target cell permissive factor required for contact-dependent growth inhibition (CDI). *Genes Dev*, **26**, 515–525.
22. Jones,A.M., Garza-Sanchez,F., So,J., Hayes,C.S. and Low,D.A. (2017) Activation of contact-dependent antibacterial tRNase toxins by translation elongation factors. *Proc. Natl. Acad. Sci. U.S.A.*, **114**, E1951–E1957.
23. Zhang,D., de Souza,R.F., Anantharaman,V., Iyer,L.M. and Aravind,L. (2012) Polymorphic toxin systems: comprehensive characterization of trafficking modes, processing, mechanisms of action, immunity and ecology using comparative genomics. *Biol. Direct.*, **7**, 18.
24. Eschenfeldt,W.H., Makowska-Grzyska,M., Stols,L., Donnelly,M.I., Jedrzejczak,R. and Joachimiak,A. (2013) New LIC vectors for production of proteins from genes containing rare codons. *J. Struct. Funct. Genomics*, **14**, 135–144.
25. Eschenfeldt,W.H., Maltseva,N., Stols,L., Donnelly,M.I., Gu,M., Nocek,B., Tan,K., Kim,Y. and Joachimiak,A. (2010) Cleavable C-terminal His-tag vectors for structure determination. *J. Struct. Funct. Genomics*, **11**, 31–39.
26. Aslanidis,C. and de Jong,P.J. (1990) Ligation-independent cloning of PCR products (LIC-PCR). *Nucleic Acids Res.*, **18**, 6069–6074.
27. Eschenfeldt,W.H., Stols,L., Millard,C.S., Joachimiak,A. and Mark,I.D. (2009) A family of LIC vectors for high-throughput cloning and purification of proteins. *Methods Mol. Biol.*, **498**, 105–115.
28. Willett,J.L., Gucinski,G.C., Fatherree,J.P., Low,D.A. and Hayes,C.S. (2015) Contact-dependent growth inhibition toxins exploit multiple independent cell-entry pathways. *Proc. Natl. Acad. Sci. U.S.A.*, **112**, 11341–11346.
29. Thomason,L., Court,D.L., Bubunenko,M., Costantino,N., Wilson,H., Datta,S. and Oppenheim,A. (2007) Recombineering: genetic engineering in bacteria using homologous recombination. *Curr. Protoc. Mol. Biol.*, doi:10.1002/0471142727.mb0116s78.
30. Stols,L., Millard,C.S., Dementieva,I. and Donnelly,M.I. (2004) Production of selenomethionine-labeled proteins in two-liter plastic bottles for structure determination. *J. Struct. Funct. Genomics*, **5**, 95–102.
31. Minor,W., Cymborowski,M., Otwinowski,Z. and Chruszcz,M. (2006) HKL-3000: the integration of data reduction and structure solution–from diffraction images to an initial model in minutes. *Acta Crystallogr. D Biol. Crystallogr.*, **62**, 859–866.
32. French,S. and Wilson,K. (1978) On the treatment of negative intensity observations. *Acta Crystallogr. A*, **A34**, 517–525.
33. Padilla,J.E. and Yeates,T.O. (2003) A statistic for local intensity differences: robustness to anisotropy and pseudo-centering and utility for detecting twinning. *Acta Crystallogr. D Biol. Crystallogr.*, **59**, 1124–1130.
34. Winn,M.D., Ballard,C.C., Cowtan,K.D., Dodson,E.J., Emsley,P., Evans,P.R., Keegan,R.M., Krissinel,E.B., Leslie,A.G., McCoy,A. *et al.* (2011) Overview of the CCP4 suite and current developments. *Acta Crystallogr. D Biol. Crystallogr.*, **67**, 235–242.
35. Karplus,P.A. and Diederichs,K. (2012) Linking crystallographic model and data quality. *Science*, **336**, 1030–1033.
36. Davis,I.W., Murray,L.W., Richardson,J.S. and Richardson,D.C. (2004) MOLPROBITY: structure validation and all-atom contact analysis for nucleic acids and their complexes. *Nucleic Acids Res.*, **32**, W615–W619.
37. Sheldrick,G.M. (2008) A short history of SHELX. *Acta Crystallogr. A*, **64**, 112–122.
38. Otwinowski,Z. (1991) Maximum likelihood refinement of heavy atom parameters. In: *Proceedings of the CCP4 Study Weekend, CCP4 Eds, 25–26 January 1991*. Daresbury Laboratory, Warrington, pp. 80–85.
39. Cowtan,K. (1994) DM: an automated procedure for phase improvement by density modification. *Joint CCP4 and ESF-EACBM newsletter on protein crystallography*. Vol. **31**, pp. 34–38.
40. Cowtan,K. (2006) The Buccaneer software for automated model building. 1. Tracing protein chains. *Acta Crystallogr. D Biol. Crystallogr.*, **62**, 1002–1011.
41. Emsley,P. and Cowtan,K. (2004) Coot: model-building tools for molecular graphics. *Acta Crystallogr. D Biol. Crystallogr.*, **60**, 2126–2132.
42. Murshudov,G.N., Vagin,A.A. and Dodson,E.J. (1997) Refinement of macromolecular structures by the maximum-likelihood method. *Acta Crystallogr. D Biol. Crystallogr.*, **53**, 240–255.
43. McCoy,A.J. (2007) Solving structures of protein complexes by molecular replacement with Phaser. *Acta Crystallogr. D Biol. Crystallogr.*, **63**, 32–41.
44. Adams,P.D., Baker,D., Brunger,A.T., Das,R., DiMaio,F., Read,R.J., Richardson,D.C., Richardson,J.S. and Terwilliger,T.C. (2013) Advances, interactions, and future developments in the CNS, Phenix, and Rosetta structural biology software systems. *Annu. Rev. Biophys.*, **42**, 265–287.
45. Terwilliger,T.C., Read,R.J., Adams,P.D., Brunger,A.T., Afonine,P.V., Grosse-Kunstleve,R.W. and Hung,L.W. (2012) Improved crystallographic models through iterated local density-guided model deformation and reciprocal-space refinement. *Acta Crystallogr. D Biol. Crystallogr.*, **68**, 861–870.
46. Nicholls,R.A., Fischer,M., McNicholas,S. and Murshudov,G.N. (2014) Conformation-independent structural comparison of macromolecules with ProSMART. *Acta Crystallogr. D Biol. Crystallogr.*, **70**, 2487–2499.
47. McGinness,K.E., Baker,T.A. and Sauer,R.T. (2006) Engineering controllable protein degradation. *Mol. Cell*, **22**, 701–707.
48. Poole,S.J., Diner,E.J., Aoki,S.K., Braaten,B.A., T'Kint de Roodenbeke,C., Low,D.A. and Hayes,C.S. (2011) Identification of functional toxin/immunity genes linked to contact-dependent growth inhibition (CDI) and rearrangement hotspot (Rhs) systems. *PLoS Genet.*, **7**, e1002217.
49. Garza-Sánchez,F., Janssen,B.D. and Hayes,C.S. (2006) Prolyl-tRNA(Pro) in the A-site of SecM-arrested ribosomes inhibits the recruitment of transfer-messenger RNA. *J. Biol. Chem.*, **281**, 34258–34268.
50. Hayes,C.S. and Sauer,R.T. (2003) Cleavage of the A site mRNA codon during ribosome pausing provides a mechanism for translational quality control. *Mol. Cell*, **12**, 903–911.
51. Jacobson,G.R. and Rosenbusch,J.P. (1977) Limited proteolysis of elongation factor Tu from Escherichia coli, Multiple intermediates. *Eur. J. Biochem.*, **77**, 409–417.
52. Arai,K., Clark,B.F., Duffy,L., Jones,M.D., Kaziro,Y., Laursen,R.A., L'Italien,J., Miller,D.L., Nagarkatti,S., Nakamura,S. *et al.* (1980) Primary structure of elongation factor Tu from Escherichia coli. *Proc. Natl. Acad. Sci. U.S.A.*, **77**, 1326–1330.
53. Nakamura,S., Arai,K., Takahashi,K. and Kaziro,Y. (1975) Amino acid sequences of two sulfhydryl-containing tryptic peptides of the polypeptide chain elongation factor Tu. *Biochem. Biophys. Res. Commun.*, **66**, 1069–1077.
54. Arai,K., Nakamura,S., Arai,T., Kawakita,M. and Kaziro,Y. (1976) Limited hydrolysis of the polypeptide chain elongation factor Tu by trypsin. Isolation and characterization of the polypeptide fragments. *J. Biochem.*, **79**, 69–83.
55. Jurnak,F., McPherson,A., Wang,A.H. and Rich,A. (1980) Biochemical and structural studies of the tetragonal crystalline modification of the *Escherichia coli* elongation factor Tu. *J. Biol. Chem.*, **255**, 6751–6757.
56. Jurnak,F., Rich,A. and Miller,D. (1977) Preliminary x-ray diffraction data for tetragonal crystals of trypsinized *Escherichia coli* elongation factor. *J. Mol. Biol.*, **115**, 103–110.
57. Krissinel,E. and Henrick,K. (2007) Inference of macromolecular assemblies from crystalline state. *J. Mol. Biol.*, **372**, 774–797.

58. Kjeldgaard,M., Nissen,P., Thirup,S. and Nyborg,J. (1993) The crystal structure of elongation factor EF-Tu from Thermus aquaticus in the GTP conformation. *Structure*, **1**, 35–50.
59. Nissen,P., Kjeldgaard,M., Thirup,S., Polekhina,G., Reshetnikova,L., Clark,B.F. and Nyborg,J. (1995) Crystal structure of the ternary complex of Phe-tRNAPhe, EF-Tu, and a GTP analog. *Science*, **270**, 1464–1472.
60. Nissen,P., Thirup,S., Kjeldgaard,M. and Nyborg,J. (1999) The crystal structure of Cys-tRNACys-EF-Tu-GDPNP reveals general and specific features in the ternary complex and in tRNA. *Structure*, **7**, 143–156.
61. Song,H., Parsons,M.R., Rowsell,S., Leonard,G. and Phillips,S.E. (1999) Crystal structure of intact elongation factor EF-Tu from *Escherichia coli* in GDP conformation at 2.05 A resolution. *J. Mol. Biol.*, **285**, 1245–1256.
62. Dong,H., Nilsson,L. and Kurland,C.G. (1996) Co-variation of tRNA abundance and codon usage in *Escherichia coli* at different growth rates. *J. Mol. Biol.*, **260**, 649–663.
63. Ruhe,Z.C., Townsley,L., Wallace,A.B., King,A., Van der Woude,M.W., Low,D.A., Yildiz,F.H. and Hayes,C.S. (2015) CdiA promotes receptor-independent intercellular adhesion. *Mol. Microbiol.*, **98**, 175–192.
64. Betat,H., Rammelt,C. and Morl,M. (2010) tRNA nucleotidyltransferases: ancient catalysts with an unusual mechanism of polymerization. *Cell Mol. Life Sci.*, **67**, 1447–1463.
65. Vorstenbosch,E., Pape,T., Rodnina,M.V., Kraal,B. and Wintermeyer,W. (1996) The G222D mutation in elongation factor Tu inhibits the codon-induced conformational changes leading to GTPase activation on the ribosome. *EMBO J.*, **15**, 6766–6774.
66. Schmeing,T.M., Voorhees,R.M., Kelley,A.C., Gao,Y.G., Murphy,F.V.t., Weir,J.R. and Ramakrishnan,V. (2009) The crystal structure of the ribosome bound to EF-Tu and aminoacyl-tRNA. *Science*, **326**, 688–694.
67. Abel,K., Yoder,M.D., Hilgenfeld,R. and Jurnak,F. (1996) An alpha to beta conformational switch in EF-Tu. *Structure*, **4**, 1153–1159.
68. Burnett,B.J., Altman,R.B., Ferguson,A., Wasserman,M.R., Zhou,Z. and Blanchard,S.C. (2014) Direct evidence of an elongation factor-Tu/Ts.GTP.Aminoacyl-tRNA quaternary complex. *J. Biol. Chem.*, **289**, 23917–23927.
69. Burnett,B.J., Altman,R.B., Ferrao,R., Alejo,J.L., Kaur,N., Kanji,J. and Blanchard,S.C. (2013) Elongation factor Ts directly facilitates the formation and disassembly of the Escherichia coli elongation factor Tu.GTP.aminoacyl-tRNA ternary complex. *J. Biol. Chem.*, **288**, 13917–13928.
70. Yikilmaz,E., Chapman,S.J., Schrader,J.M. and Uhlenbeck,O.C. (2014) The interface between Escherichia coli elongation factor Tu and aminoacyl-tRNA. *Biochemistry*, **53**, 5710–5720.
71. Vorstenbosch,E.L., Potapov,A.P., de Graaf,J.M. and Kraal,B. (2000) The effect of mutations in EF-Tu on its affinity for tRNA as measured by two novel and independent methods of general applicability. *J. Biochem. Biophys. Methods*, **42**, 1–14.
72. Roy,H. and Ibba,M. (2008) RNA-dependent lipid remodeling by bacterial multiple peptide resistance factors. *Proc. Natl. Acad. Sci. U.S.A.*, **105**, 4667–4672.
73. Furano,A.V. (1975) Content of elongation factor Tu in *Escherichia coli*. *Proc. Natl. Acad. Sci. U.S.A.*, **72**, 4780–4784.
74. Webb,J.S., Nikolakakis,K.C., Willett,J.L., Aoki,S.K., Hayes,C.S. and Low,D.A. (2013) Delivery of CdiA nuclease toxins into target cells during contact-dependent growth inhibition. *PLoS One*, **8**, e57609.
75. Zhang,D., Iyer,L.M. and Aravind,L. (2011) A novel immunity system for bacterial nucleic acid degrading toxins and its recruitment in various eukaryotic and DNA viral systems. *Nucleic Acids Res.*, **39**, 4532–4552.
76. Feng,S., Chen,Y., Kamada,K., Wang,H., Tang,K., Wang,M. and Gao,Y.G. (2013) YoeB-ribosome structure: a canonical RNase that requires the ribosome for its specific activity. *Nucleic Acids Res.*, **41**, 9549–9556.
77. Pedersen,K., Zavialov,A.V., Pavlov,M.Y., Elf,J., Gerdes,K. and Ehrenberg,M. (2003) The bacterial toxin RelE displays codon-specific cleavage of mRNAs in the ribosomal A site. *Cell*, **112**, 131–140.
78. Heaton,B.E., Herrou,J., Blackwell,A.E., Wysocki,V.H. and Crosson,S. (2012) Molecular structure and function of the novel BrnT/BrnA toxin-antitoxin system of Brucella abortus. *J. Biol. Chem.*, **287**, 12098–12110.
79. Yamaguchi,Y., Park,J.H. and Inouye,M. (2011) Toxin-antitoxin systems in bacteria and archaea. *Annu. Rev. Genet.*, **45**, 61–79.
80. Gerdes,K. and Maisonneuve,E. (2012) Bacterial persistence and toxin-antitoxin loci. *Annu. Rev. Microbiol.*, **66**, 103–123.
81. Harms,A., Maisonneuve,E. and Gerdes,K. (2016) Mechanisms of bacterial persistence during stress and antibiotic exposure. *Science*, **354**, aaf4268.
82. Garcia,E.C., Perault,A.I., Marlatt,S.A. and Cotter,P.A. (2016) Interbacterial signaling via *Burkholderia* contact-dependent growth inhibition system proteins. *Proc. Natl. Acad. Sci. U.S.A.*, **113**, 8296–8301.